OBSERVATIONS ON ATMOSPHERIC NEUTRINOS WITH SOUDAN 2

ANTHONY MANN, TOMAS KAFKA, and MAYLY SANCHEZ

Department of Physics, Tufts University
Medford, MA 02155, U.S.A.

for

The Soudan 2 Collaboration
Argonne - Minnesota - Oxford - Rutherford Appleton - Tufts - W. Washington

ABSTRACT

Using contained track and shower events from a 4.2-kty exposure we find an atmospheric neutrino flavor ratio-of-ratios which is anomalous: $R = 0.66 \pm 0.11 \pm 0.06$. To investigate the anomaly's probable origin with ν_μ to ν_x oscillations, we utilize samples of contained and partially contained events selected for good resolution in reconstructing the incident neutrino direction. By minimizing χ^2 for data events versus oscillation-weighted MC events in bins of $\log(L/E_\nu)$ ($\log(L/E_{vis})$) for contained (partially contained) ν_μ events, we obtain at χ^2_{min} + 4.61: $0.68 < \sin^2\theta \leq 1.0$ and $2 \times 10^{-3} < \Delta m^2 < 3 \times 10^{-2}$ eV^2.

1. Introduction

The Soudan 2 detector is a fine-grained iron tracking calorimeter which has been taking data since April 1989; it is operating underground at a depth of 2100 meters-water-equivalent on level 27 of the Soudan Mine Underground State Park in northern Minnesota.

The detector operates as a slow-drift time projection chamber. Its basic charged particle detection elements are 1 meter long, slightly conductive, hytrel plastic drift tubes. These are sandwiched between mylar sheets so as to comprise a "bandolier" assembly of tubes; a bandolier is interleaved with corrugated steel sheets to form a massive stack of honeycomb geometry. A stack is packaged with wireplanes and cathode pickup strips at the drift tube ends and surrounded on all sides by thin-steel side skins which provide the gas seal. The resulting assemblies are standard-unit calorimeter modules, each 4.3 metric tons in mass.[1] The tracking calorimeter is constructed building-block fashion out of two-layer 'walls', eight modules wide each. The fourteen walls of calorimeter modules form the compact, dense Central Detector having a mass of 963 metric tons. The calorimeter is surrounded on all sides by a double-layer, cavern-liner proportional tube Active Shield of 1700 m^2 total tracking area.[2]

Figure 1 shows the vertex region of a contained event recorded by the tracking calorimeter, viewed from the top, side, and front of the detector. The event is a two-prong and is a candidate quasi-elastic interaction, $\nu\ n \rightarrow \mu^-\ p$. The two tracks have ionization signatures which result from pulse height dE/dx sampling: The shorter

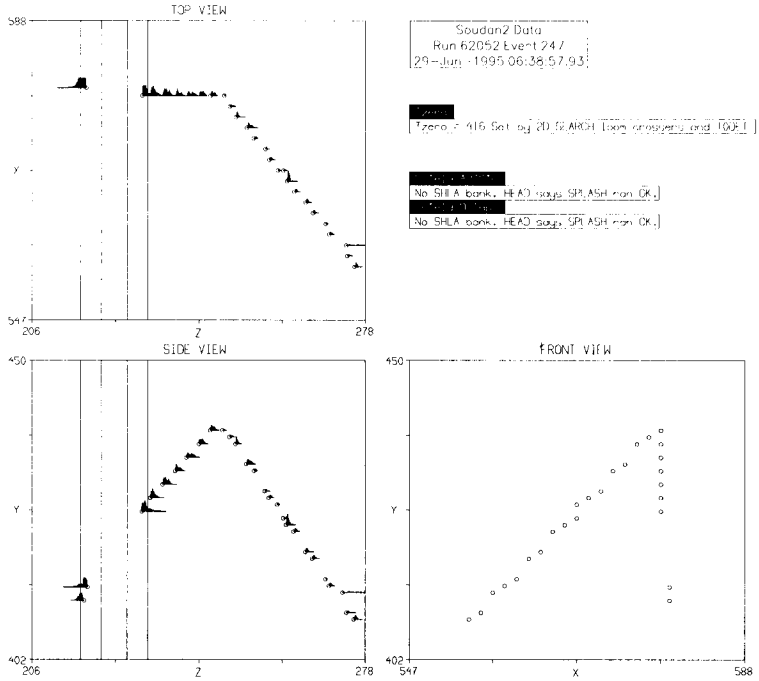

Fig. 1. Vertex region of a contained two-prong event; ionization and multiple scattering distinguish the proton from the muon track.

track is very straight and heavily ionizing - typical of a proton; in contrast, the candidate muon track is relatively lightly ionizing and exhibits multiple scattering.

An energetic contained multiprong event is shown in Fig. 2. The neutrino flavor of the event is clear since it has a leading prong which is a muon. The muon has a visible endpoint decay; consequently it is more probably a μ^+ than a μ^-, since the latter usually undergo nuclear absorption at endpoint in the calorimeter's iron medium. For multiprongs of lower visible energy, flavor-tagging can be more problematic.

2. The Neutrino Flavor Ratio

In addition to neutrino interactions, Soudan 2 contained event (CEV) samples also include background reactions. The latter arise from inelastic interactions of cosmic ray muons with nuclei within the cavern rock that surrounds the detector. These interactions can give rise to energetic photons and neutrons which enter the cavern and initiate interaction/conversion topologies which appear contained in the central detector. In most interactions of this kind, the muon also enters and traverses the cavern, giving rise to coincident hits on opposing surfaces of the active shield. Additionally, these deep inelastic muon reactions often produce a spray of charged secondary particles which produce hits in the shield. From among these shield-tagged "rock events", we retain those having more than one time-coincident shield hit as a background control sample. In our CEV samples for which there are zero associated

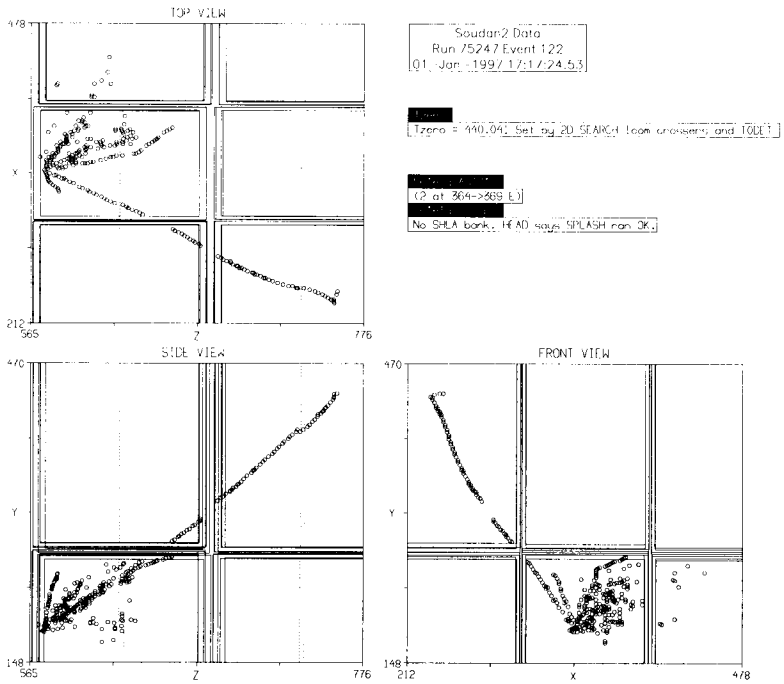

Fig. 2. An energetic contained multiprong event. The leading non-scattering prong is a muon track (a likely μ^+), consequently the event is assigned a ν_μ flavor.

shield hits (so-called "gold" events) and which are mostly neutrino events, one has to account for contaminant rock events which did not fire the shield, either because of shield inefficiency or because there were in fact no charged particle companions to the neutron or photon which entered the cavern. To estimate the amount of this residual rock background, we rely on fitting of the gold data vertex depth (taken to be the shortest distance from vertex to the detector exterior) to the sum of the expected neutrino distribution (from our full-simulation Monte Carlo) plus the background depth distribution (from the shield-tagged rock data). With the rock background estimates in hand, we correct the populations of our single track and shower samples and obtain the numbers of neutrino-induced tracks and showers. The ratio of track to shower events thus obtained, comprises our best determination of the atmospheric ν_μ/ν_e flavor ratio.

The event populations of Table 1 are used to calculate the flavor ratio-of-ratios observed in Soudan 2. From an exposure of 4.2 fiducial kiloton-years (kty) which is an update on our result at 3.9 kty recently published,[3] we obtain

$$R = 0.66 \pm 0.11(stat) \pm 0.06(syst). \quad (1)$$

Our result, which is based upon predominantly sub-GeV events, is anomalous relative

Table 1. Atmospheric neutrino flavor ratio from 4.2 fiducial kiloton-years.

Number of Gold Tracks	105
Number of Gold Showers	159
Number of MC Tracks	847 (155.4)
Number of MC Showers	805 (147.7)
Corrected Number of ν Tracks	83.6 ± 11.2
Corrected Number of ν Showers	119.7 ± 12.9
Corrected Value of R	0.66 ± 0.11

to the expectation of $R = 1.0$ from neutrino physics without oscillations.

3. Electron- and Muon-Neutrino High Resolution Samples

To see how neutrino oscillations can cause the flavor anomaly, we turn to the phenomenology for two-state mixing, $\nu_\mu \leftrightarrow \nu_x$, which gives the well-known oscillation survival probability formula

$$P(\nu_\mu \rightarrow \nu_\mu) \;=\; 1 - \sin^2 2\theta \, \sin^2 \left(\frac{1.267 \Delta m^2 L}{E_\nu} \right) . \qquad (2)$$

Since the oscillation probability is a function of L/E_ν, and since both L and E_ν can be measured event-by-event in Soudan 2, we are motivated to analyze our data in terms of L/E_ν - or, more conveniently, $\log_{10}(L/E_\nu)$. In a fine-grained tracking calorimeter, measurement of E_ν is straightforward, E_ν being the sum of individual energies of all final-state tracks and showers. However, L/E_ν also requires good determination of L calculated from the reconstructed zenith angle of the event. A respectable resolution for the neutrino direction can be achieved at sub-GeV energies, even down to threshold energies, provided that the recoil hadronic system is fully imaged. As summarized in Table 2, for quasi-elastic reactions $\nu_\ell \; n \rightarrow \ell \; p$, if only the final-state lepton is imaged, the determination of the incident neutrino direction is poor ($\Delta\theta(\nu \cdot lepton) > 50^\circ$) for events having E_{lept} below 600 MeV; but such events comprise the major portion of sub-GeV samples. One only recovers a respectable resolution for the neutrino direction by going to higher energy events ($E_{lept} > 600$ MeV).

However, if the final state recoil proton is also imaged and reconstructed along with the lepton, then a useful degree of angular resolution is recovered even down to the threshold, as indicated in the lower row of Table 2.

We therefore devised a set of selections, to be applied to Soudan 2 gold data events, which isolate samples of ν_μ- and ν_e-flavor charged current events having good resolution for neutrino pointing. From among the (predominantly) quasi-elastic single track and shower events, we retain those having measurable recoil protons; otherwise, if a recoil is absent, we require the lepton energy to exceed 600 MeV. We also select

Table 2. Angular resolution for quasi-elastic events.

E_{lept} (MeV)	0-200	200-400	400-600	>600
$\overline{\Delta\theta}(\nu$-lepton)	$\sim 90°$	75°	49°	28°
$\overline{\Delta\theta}(\nu$-lepton+rec)	30°	23°	15°	8°

multiprong events, but require E_{vis} to exceed 700 MeV and the vector sum of all visible-prong momenta to exceed 450 MeV/c. To ensure reliable flavor-tagging (success probability > 0.92), the candidate lepton prong (leading, prompt prong from the vertex, devoid of hadronic scatter) is required to have momentum above 250 MeV/c. The resolution obtained with samples satisfying these cuts is displayed in Table 3. The neutrino direction is on average determined to 20-30 degrees, with event $\Delta E/E$ about 20%.

Table 3. Resolution in kinematic variables for the HiRes samples.

Variable	Quantity	ν_μ CC	ν_e CC
Energy	$\Delta E/E$	20%	23%
Angle	$\angle\vec{p}_\nu(true)\cdot\vec{p}_\nu(recon)$	33.2°	21.3°
L/E	$\lvert\log(trueL/E)-\log(reconL/E)\rvert$	0.49	0.43

Table 4 summarizes the "high resolution" (HiRes) event samples obtained from an exposure of 4.4 kty. Included in these samples are Soudan's first-time utilization of multiprong events for which one track stops on an interior crack of the detector, and also a few energetic multiprongs for which the primary vertex is in an interior non-active region (e.g. vertex is in a module load plate or side skin). The latter topologies comprise 8.4% of the total samples.

Table 4. High resolution event samples, 4.4 kty. The Monte Carlo rates are normalized to the HiRes ν_e data sample.

Category	*Data*		*MC*
	Before bgr. subtraction	*After bgr. subtraction*	*normalized*
Tracks	54.0 ± 7.3	47.7 ± 7.4	102.5 ± 4.1
Showers	77.0 ± 8.8	73.8 ± 8.8	71.9 ± 3.4
MP, ν_μ	39.0 ± 6.2	37.6 ± 6.7	41.9 ± 2.6
MP, ν_e	44.0 ± 6.6	41.7 ± 6.7	43.6 ± 2.6
ν_μ		85.4 ± 9.7	144.4 ± 4.8
ν_e		115.6 ± 11.1	115.6 ± 4.3

Combining the sample of track events (47.7 events after rock subtraction), with the ν_μ-flavor multiprongs (37.6 events), we obtain a total of 85.4 ν_μ events of good

resolution. Similarly, we obtain from the shower events plus the ν_e multiprongs, a total of 115.6 good resolution ν_e events. Event rates obtained via processing Monte Carlo events in the same way as the data, are displayed in the third column of Table 4. The Monte Carlo is a full simulation of detector responses which produces data-like events; these are injected into the data stream in front of all scanning and are processed "blind" along with the data, to be separated out only after gold samples have been isolated. Our Monte Carlo is based upon Bartol neutrino fluxes [4)5)] and standard physics without neutrino oscillations.[6)]

After normalization of the Monte Carlo to the 4.4 kty exposure, we find the expected ν_e rates to exceed our observed event rates. In Table 4 and also in histogrammed distributions of Monte Carlo events to follow, we have normalized the MC rates to that observed for the high resolution ν_e sample. This is implemented by applying an overall factor of 0.86 to the MC rates and amounts to a lowering of the Bartol absolute fluxes.

From the MC ν_μ versus ν_e rates (lower right-hand column of Table 4), it is seen that ν_μ events are expected to exceed ν_e's, whereas the opposite is found with data. The ratio-of-ratios observed with our high resolution samples is $R = 0.59 \pm 0.09$ (statistical error only), which is also significantly below 1.0. The rock event background subtractions are relatively modest for these samples ($\sim$ 5%). This happens because event E_{vis} values are higher on average than for the single track and shower samples, and the rock backgrounds are predominantly of low energy.

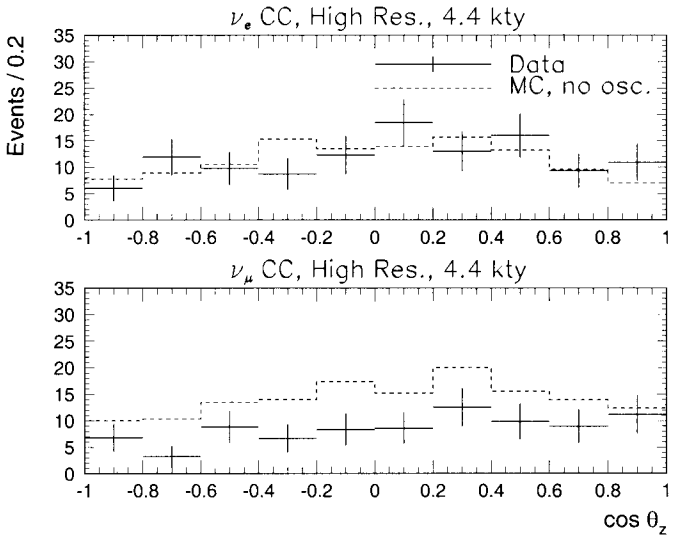

Fig. 3. Distributions in $\cos\theta_z$ for HiRes ν_e and ν_μ flavor event samples. Data (crosses) are compared with the no-oscillation MC (dashed histograms).

The zenith angle distributions for the HiRes ν_μ and ν_e samples are shown in Figs. 3a,b. In these Figures $\cos\ \theta_z = 1.0$ corresponds to neutrino incident from directly overhead. For the ν_e sample, the zenith angle distribution follows the shape expected from the Monte Carlo without oscillations. In contrast, zenith angles for the

ν_μ sample exhibit a dearth of events at all directions with the possible exception of the flux at highest zenith values. Unfortunately, the modest statistics of our currently available HiRes CEV ν_μ sample precludes any strong statement as to whether there exists an up-down asymmetry of same sign as reported in the SuperKamiokande sub-GeV data (fewer up-going than down-going events).

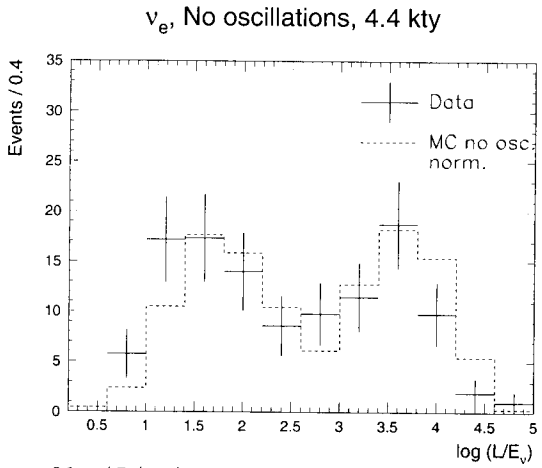

Fig. 4. Distribution of $\log(L/E_\nu)$ for ν_e charged-current events (crosses) compared to the neutrino MC with no oscillations.

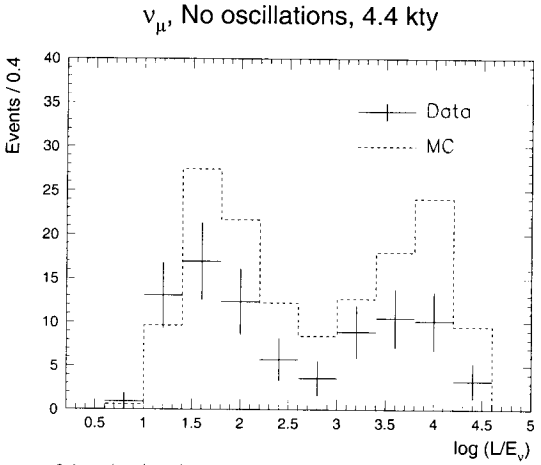

Fig. 5. Distribution of $\log(L/E_\nu)$ for ν_μ events; relative to no-oscillation expectation, a dearth exists for all but the most downward-going events.

We now examine the $\log(L/E_\nu)$ data distributions for the high resolution event samples. Fig. 4 depicts L/E_ν for the ν_e events. The data is observed to follow the no-oscillation MC expectation reasonably although not superbly - the χ^2 per degree of freedom is about 1.5. There is however no suggestion of distortion in either hemisphere, and the central dip at the horizon is evident. In contrast, the $\log(L/E_\nu)$

distribution of ν_μ events shown in Fig. 5 exhibits a clear depletion of the up-going flux and of the flux through the horizon region. Depletion of ν_μ's is also seen in the the down-going flux for $\log(L/E_\nu)$ above 1.5 (L/E in km/GeV).

Before searching for the "best" ν_μ - ν_x mixing parameters, we consider some exploratory match-ups of neutrino oscillation solutions to the ν_μ data binned in $\log(L/E_\nu)$. Setting $\sin^2 2\theta$ to unity, we compare the ν_μ data to the expectation (obtained by weighting the Monte Carlo events) for two-state neutrino oscillations with $\Delta m^2 = 10^{-4}$ eV^2, as shown in Fig. 6a. With these parameter settings, the oscillation solution allows too many ν_μ's to survive, particularly in the downward flux through the horizon in the $\log(L/E_\nu)$ region 1.5 to 3.0. With $\Delta m^2 = 10^{-3}$ eV^2 shown in Fig. 6b, agreement for the upward flux ($\log(L/E_\nu) > 3.0$) is good, but the prediction still exceeds the data for a portion of the downward flux. Going to still higher Δm^2, we find a good match over the full $\log(L/E_\nu)$ range with $\Delta m^2 = 9 \times 10^{-3}$ eV^2 (Fig. 6c). At $\Delta m^2 = 10^{-1}$ eV^2 however (Fig. 6d), the prediction from two-state oscillations appears depleted in the more vertical downward flux.

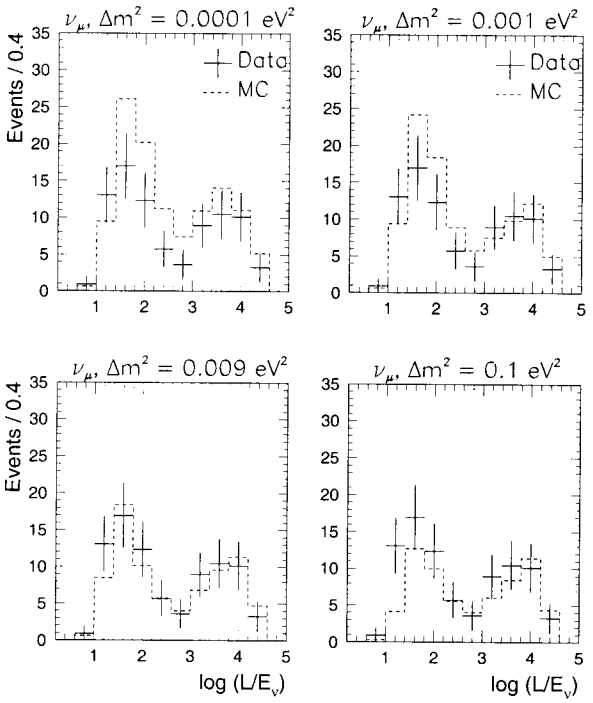

Fig. 6. Comparison of L/E_ν distribution for ν_μ data (crosses) and expectations from neutrino oscillations for four Δm^2 values, with $\sin^2 2\theta = 1.0$.

To determine Δm^2 and $\sin^2 2\theta$ from our fully contained HiRes ν_μ events, we fit the atmospheric neutrino Monte Carlo distribution, including the effects of neutrino oscillations, to the data L/E_ν distribution corrected for the rock background. We assume that no neutrino oscillations occur in the ν_e flux, and include the rate of HiRes ν_e events as a term in the total χ^2:

$$\chi^2_{ijk} = \sum_{\nu_\mu} \frac{[Data(\frac{L(\bar{h})}{E}) - f_{\nu k} \times f_{MC} \times \int dh\ w_{ij}(\frac{L(h)}{E})]^2}{[Error(Data)]^2} + \frac{[\sum \nu_e Data - f_{\nu k} \times f_{MC} \times \sum \nu_e MC]^2}{[Error(\sum \nu_e Data)]^2} \quad (3)$$

Here, f_{MC} is the ratio of data exposure to MC exposure, which is $(5.45)^{-1}$. In addition to the oscillation parameters Δm^2 and $\sin^2 2\theta$, the fit is allowed to vary the overall normalization of data and MC via the parameter f_ν. The fit parameters are varied over the ranges $10^{-4} < \Delta m^2 < 0.5$ eV^2, $0 < \sin^2 2\theta < 1.3$, and $0.65 < f_\nu < 1.0$. For the mixing angle, values $\sin^2 2\theta > 1$ are of course unphysical, and it is not clear what χ^2 values mean in such a domain. Nevertheless, we prefer to let the χ^2 find its own minimum. As it turns out, the χ^2 finds a shallow minimum extending into $\sin^2 2\theta$ slightly greater than 1.0 but exhibits no tendency to go higher. The minimum occurs at $\Delta m^2 = 9.0 \times 10^{-3}$ eV^2 and $\sin^2 2\theta = 1.06$, with $f_\nu = 0.87$.

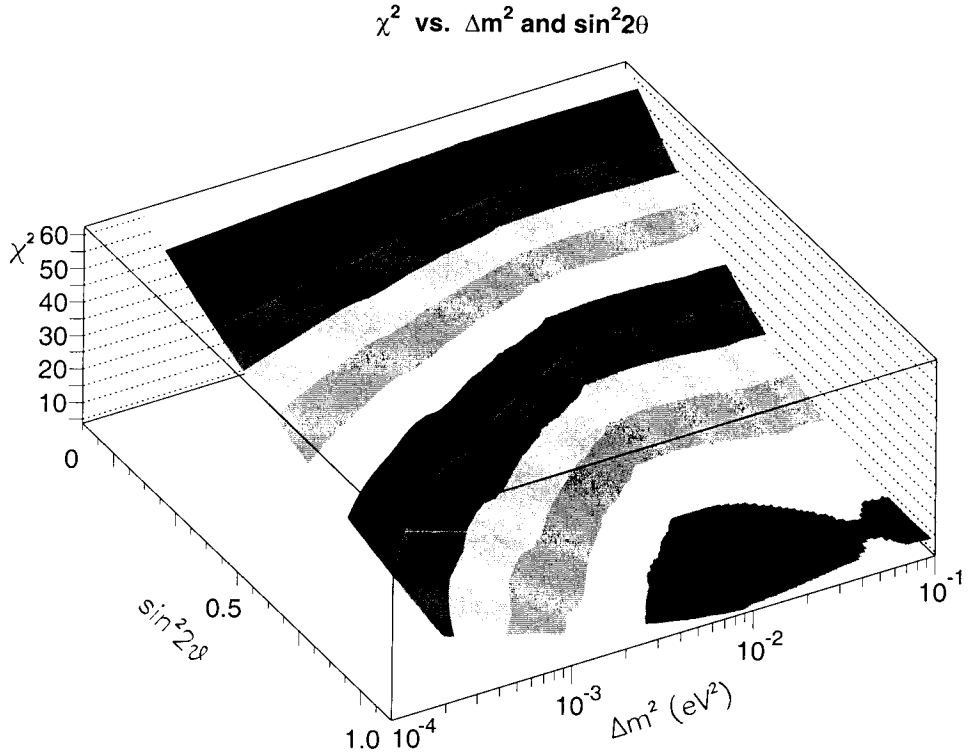

Fig. 7. χ^2 over the Δm^2, $\sin^2 2\theta$ plane from the fit of Eq. (4) wherein the MC normalization was allowed to float. Boundaries of shaded bands at increasing χ^2 correspond to $\chi^2_{min} + N \times 4.61$. The lowest-lying shaded region ($N = 1$) denotes parameters allowed by our fit at approx. 90% CL.

Fig. 7 displays the χ^2 contour surface over the Δm^2 and $\sin^2 2\theta$ plane, with f_ν set

to 0.87. The contour boundaries delineate χ^2 regions defined by

$$\chi^2_{min} + 4.61 \times N, \text{where } N = 1, 2, 3... \quad (4)$$

The lowest-lying contour region which extends along high $\sin^2 2\theta$ from $\Delta m^2 > 2 \times 10^{-3}$ eV^2 and remains open to Δm^2 values exceeding 10^{-1} eV^2, is a rough measure of the parameters allowed by the data at 90% CL. To improve our parameter determination, we turn to our sample of energetic ν_μ events which are partially contained within the tracking calorimeter.

4. Partially Contained ν_μ CC Events

Very recently, a sample of neutrino events which are partially contained within the Soudan tracking calorimeter, has been isolated. In partially contained events (PCE), the primary vertex and all or most of the final state hadronic prongs are contained within the fiducial volume, however the lepton prong exits the detector. To extract PCEs, all triggered data from the initial 4.2 kty exposure was reprocessed through a new software filter that allows events to have prongs traversing the outer fiducial volume. Approximately 15,000 events passed the new filter which had previously been rejected by our contained event filters. These events, which represent a mixture of data and Monte Carlo, have to date been single-scanned by physicists; second scanning is underway.

For the analysis reported here, we require neutrino PCE events to satisfy our HiRes event selections - the same as invoked previously for HiRes CEVs. For two-prong PCEs, there arises an abundant background from incoming cosmic ray muons which range to stopping in the detector and have end point decays. In rare instances the decays can mimic production proton or short pion tracks. To eliminate remnant muon background in two-prongs which are not recognized by ranging-to-stopping signatures, we require the shorter prong to have more than ten hits (tube crossings). This cut is quite effective, since muon endpoint decays appear as small showers which almost never exceed six hits. For gold neutrino ν_μ events of PCE type, shield hits coincident with event times are allowed, however the hits must be associated (by spatial alignment) with an exiting prong.

Using these selections we have isolated 40 ν_μ-flavor gold data events and 264 gold Monte Carlo events. From the MC sample we find that ν_μ flavor is correctly assigned in 96% of events. The rock event background in the data sample is estimated to be ≤ 1 event and is hereafter neglected.

We have used the vector sum of final state momenta as the measure of incident neutrino direction. The angle between the "true" incoming ν and the total visible momentum for our MC sample is 14 degrees on average. Comparing with the mean angular separations of Table 3, the neutrino direction determination afforded by PCEs is seen to be superior to that obtained with the HiRes CEV samples. The energies

E_ν of neutrinos which give rise to Soudan-2 PCEs can be explored using our Monte Carlo sample. The E_ν distribution of PCEs has a mean of 3.85 GeV, to be compared to 1.20 GeV for the CEVs; the distribution extends from about 1 GeV up to 10 GeV.

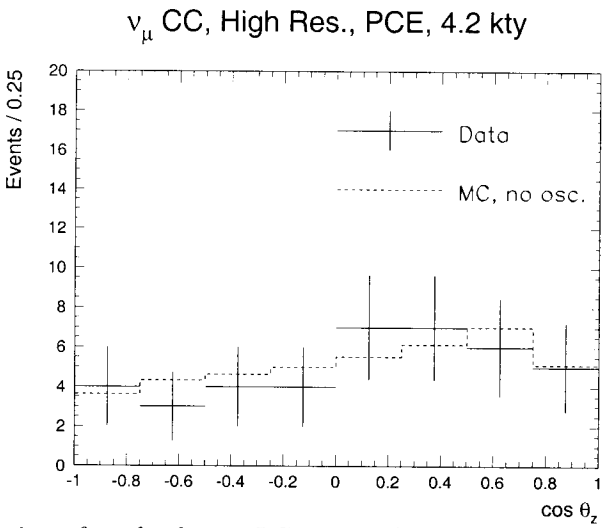

Fig. 8. Distribution of $\cos\theta_z$, for ν_μ PCE, data (crosses) versus the no-oscillation Monte Carlo (dashed histogram).

The zenith angle distribution for the 40 ν_μ data events from a 4.2 kty exposure is shown in Fig. 8. The prediction from the Monte Carlo sample for no oscillations is also shown (dashed histogram). To first order, the data agrees with the no-oscillation MC in rate (40 events versus 41 expected) and in shape. On the other hand, considering the binned data for ν_μ's from directly overhead ($\cos\theta_z = 1$) down to the horizon ($\cos\theta_z = 0$), and then moving below horizon (negative zenith-cosine), there is - optimistically perhaps - a hint of a flux step-down.

Since an energetic prong, usually the final state muon, exits the detector, the E_ν of a PCE cannot be directly measured. As an estimator which is typically lower than E_ν by $\sim 40\%$, we use the visible final state energy E_{vis}. The data and MC expectation can then be plotted in $\log(L/E_{vis})$, as shown in Fig. 9.

5. Oscillation Parameters from Soudan Data

Our χ^2 fit for $\nu_\mu - \nu_x$ oscillation parameters, which used $\log(L/E_\nu)$ bins of fully contained ν_μ events, can now be expanded. To our previous χ^2 sum we add the ν_μ PCE events binned in $\log(L/E_{vis})$ as in Fig. 9 (but with neighboring bins combined to ensure ≥ 5 events per bin).

As with previous fitting, we map the χ^2 by varying the oscillation parameters Δm^2, $\sin^2 2\theta$, and also the overall data to MC normalization f_ν. A somewhat shallow

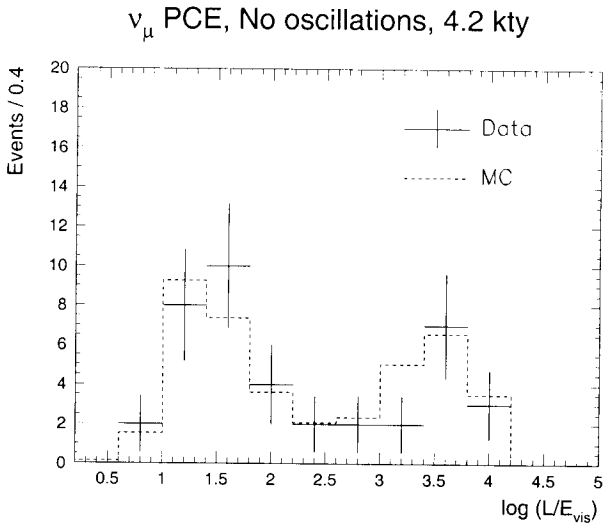

Fig. 9. Distribution of $\log(L/E_{vis})$ for ν_μ PCE events, data (crosses) versus the no-oscillation MC (dashed histogram).

but well-defined χ^2 minimum is obtained at

$$\Delta m^2 = 8.8 \times 10^{-3}\text{eV}^2 \quad \text{and} \quad \sin^2 2\theta = 1.0, \quad \text{with } f_\nu = 0.88\ . \tag{5}$$

The χ^2 surface over the $\sin^2 2\theta$ - Δm^2 plane, with f_ν fixed at the χ^2_{min} value, is shown in Fig. 10. The border of the shaded region of lowest elevation in the surface corresponds to $\chi^2_{min} + 4.61$. Comparing this allowed region for oscillations with the corresponding region in Fig. 7, the benefit arising from inclusion of the PCE sample is readily discerned. From our CEVs only, the Soudan allowed region is open to higher Δm^2 values, extending to and above 10^{-1} eV^2. In Fig. 10 however, the allowed region is now closed off to Δm^2 above $\sim 3 \times 10^{-2}$ eV^2 for all values of $\sin^2 2\theta$. For the lowest allowed Δm^2 however, the fit of Fig. 10 exhibits little change from its predecessor; Δm^2 values below 2×10^{-3} eV^2 remain disfavored.

Fig. 11 shows the regions of oscillation parameters at 68% and 90% CL which were obtained from previous smaller CEV samples via a maximum likelihood fit.[7)]

The region allowed at 90% CL by our current data smaples is contained within the dashed boundary depicted in Fig. 11, which represents the projection of the $\chi^2_{min} + 4.61$ border in Fig. 10. The new allowed region, being closed to Δm^2 above few times 10^{-2} eV^2, is more restrictive than our earlier determinations, reflecting constraints introduced by new data.

6. Summary

Using samples of fully contained single track and shower events from a 4.2-kty exposure, we obtain an atmospheric neutrino flavor ratio-of-ratios which is anomalous,

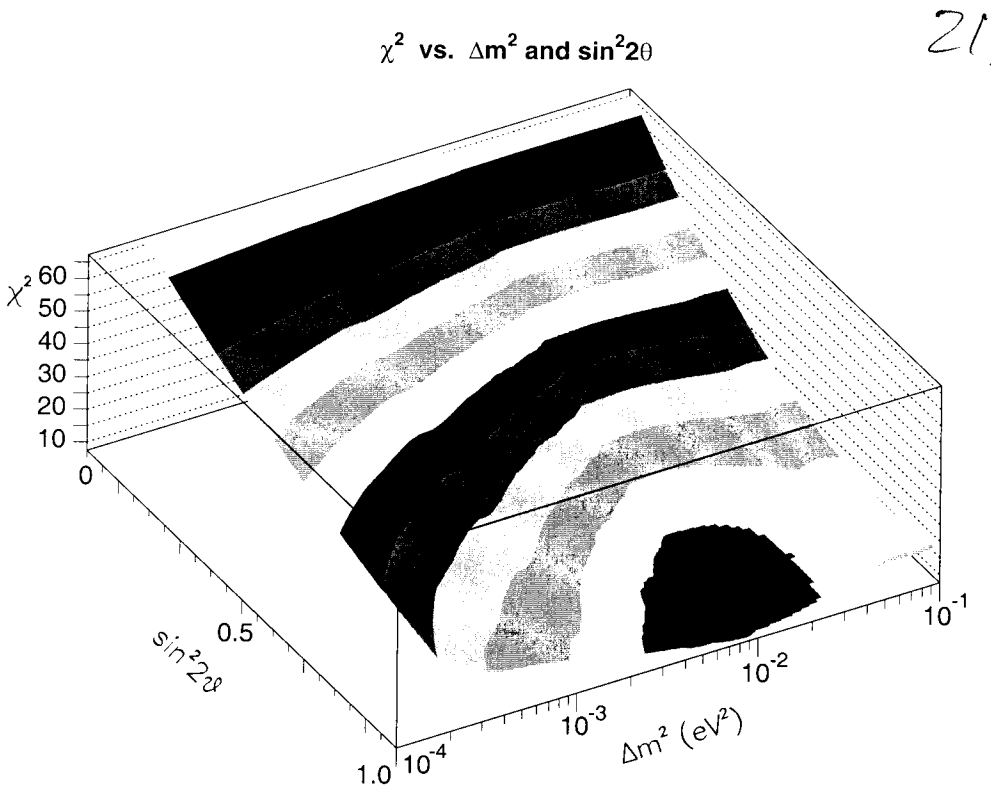

Fig. 10. χ^2 over the Δm^2, $\sin^2 2\theta$ plane from the fit of Eq. (4) but with the PCE data in bins of $\log(L/E_{vis})$ included as added terms. Addition of the PCEs results in isolation of the allowed region from parameter settings having $\Delta m^2 > 3 \times 10^{-2}$ eV^2.

$R = 0.66 \pm 0.11 \pm 0.06$. This result is an update of our published measurement based upon 3.9 kty.[3)]

To investigate the probable origin of the R anomaly with neutrino oscillations ν_μ to ν_x, we utilize samples of flavor-tagged, contained and partially contained events which are selected for good resolution in reconstructing the incident neutrino direction. By minimizing the χ^2 for data events versus oscillation-weighted MC events in bins of $\log(L/E_\nu)$ for ν_μ CEVs and in $\log(L/E_{vis})$ for ν_μ PCEs, we obtain at $\chi^2_{min} + 4.61$ (90% CL):

$$0.68 < \sin^2 2\theta \leq 1.0 \quad \text{and} \quad 2 \times 10^{-3} < \Delta m^2 < 3 \times 10^{-2} \text{eV}^2 \tag{6}$$

with the overall normalization of data to MC set to the value at χ^2_{min} of 0.88×MC (Bartol fluxes).

7. References

1) W.W.M. Allison *et al.*, *Nucl. Instr. Meth.* **A376** (1996) 36; *ibid*, **A381** (1996) 385.

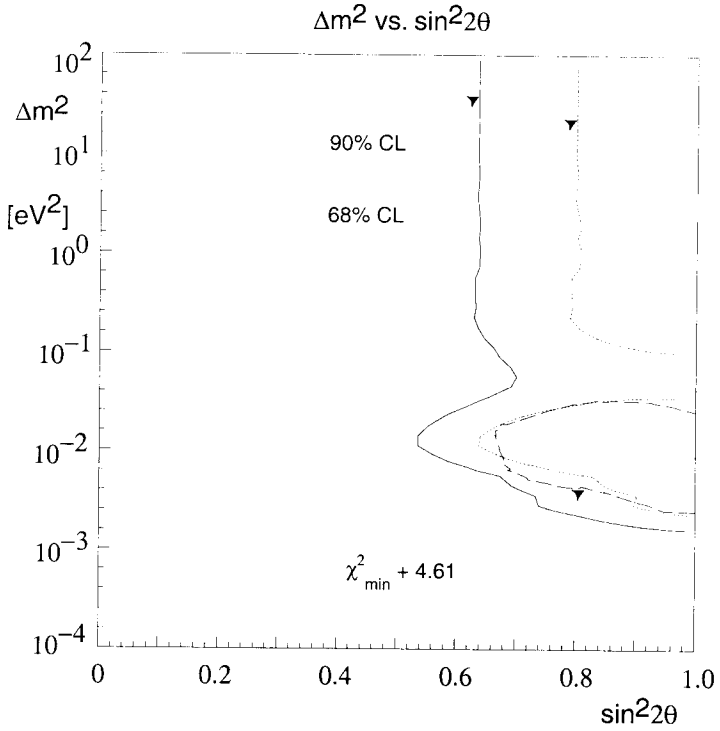

Fig. 11. Soudan-2 allowed regions (to the right of boundary curves) for $\nu_\mu \rightarrow \nu_x$ oscillations. The solid (dotted) boundary delimits regions allowed at 90% (68%) CL obtained with a Bayesian likelihood fit to an earlier data set[7]. The hand-drawn dashed curve depicts $\chi^2_{min} + 4.61$ from the fit to HiRes CEV and PCE samples of this analysis.

2) W.P. Oliver *et al.*, *Nucl. Instr. Meth.* **A276** (1989) 371.
3) W.W.M. Allison *et al.*, *Phys. Lett.* **B449** (1999) 137.
4) T.K. Gaisser, T. Stanev, and G. Barr, *Phys. Rev.* **D38** (1988) 85.
5) G. Barr, T.K. Gaisser, and T. Stanev, *Phys. Rev.* **D39** (1989) 3532.
6) W.W.M. Allison *et al.*, *Phys. Lett.* **B391** (1997) 491.
7) H. Gallagher, "Atmospheric neutrino studies in Soudan 2", to appear in the *Proceedings of the Int. Conf. on High Energy Physics ICHEP98, Vancouver, Canada, July 1998.*